JOURNAL OF SOLID STATE CHEMISTRY 112, 45–52 (1994)

Synthesis, Crystal Structure, and Thermal Behavior of Cerium(IV) Oxide Nitrate $Ce_2O(NO_3)_6(H_2O)_6 \cdot 2H_2O$

N. Guillou, J. P. Auffrédic, and D. Louër

Laboratoire de Cristallochimie (URA CNRS 1495), Université de Rennes I, Avenue du Général Leclerc, 35042 Rennes cedex, France

Received July 1, 1993; in revised form October 14, 1993; accepted October 22, 1993

A new cerium(IV) oxide nitrate, $Ce_2O(NO_3)_6(H_2O)_6 \cdot 2H_2O$, was synthesized from the dissolution in nitric acid of hydrous ceria with high specific area. Its crystal structure was determined from three-dimensional X-ray diffraction data. Crystals are monoclinic, space group $P2_1/c$, with $a = 8.7233(8)$, $b = 8.9397(8)$, $c = 13.981(1)$ Å, $\beta = 94.909(7)°$, and $Z = 2$. Full matrix least-squares techniques led to a conventional R factor of 0.023 for 2091 observed reflections. The structure consists of dimer units with formula $Ce_2O(NO_3)_6(H_2O)_6$, which are formed by two equivalent 10-fold cerium(IV) polyhedra connected by an oxo bridge. Additional water molecules are located between these units. Hydrogen bonds ensure the continuity of the structure. The thermal decomposition under vacuum of this compound was investigated by means of sequential thermodiffractometry. Two new phases, $Ce_2O(NO_3)_6 \cdot 3H_2O$ and $Ce_2O(NO_3)_6$, were identified and finely dispersed CeO_2 powder was obtained at low temperature (180°C). The microstructural features of the oxide annealed at 600°C were also studied, showing the "isotropic" shape of the crystallites.

INTRODUCTION

Although cerium(IV) is a well-known lanthanide species with a 4^+ oxidation state stable to exist in aqueous solution (see, for example, Ref. 1) as well as in solid compounds; very few data have been reported for simple combinations with nitrate groups. Indeed, only two chemical formula of cerium(IV) nitrates were reported long ago (2, 3), but no structure solution has been described while structures of related compounds with sulfate groups are known (4–8). Owing to the technological importance of "ceria" CeO_2, e.g., as active material in catalytic converters (9, 10), the preparation of monodispersed oxide particles by thermal hydrolysis of acidic solutions of cerium IV salts has been thoroughly investigated (1). Another route of interest for obtaining highly divided oxides is the use of precursors having a low thermal stability. It is the case for precursors containing nitrates, or oxalates, giving oxides with nano scale particles from thermal decomposition carried out with optimum monitoring of the solid state reactions. This has been clearly shown for zinc oxide obtained by thermal decomposition of zinc hydroxide nitrate (11) and zinc oxalate (12). In these studies the microstructure of the oxides was characterized from a careful diffraction line-broadening analysis.

In the course of the study of the CeO_2–HNO_3–H_2O system, we recently reported the crystal structure of a new hydronium cerium(III) nitrate hydrate (13). By using a similar method of synthesis, in which the reduction of Ce^{4+} into Ce^{3+} was prevented, we have been able to synthesize a new cerium(IV) nitrate compound. The single crystal structure determination, reported here, demonstrates that this compound is an oxide nitrate hydrate, $Ce_2O(NO_3)_6(H_2O)_6 \cdot 2H_2O$. Its thermal behavior and the microstructural features of the decomposition product are described.

EXPERIMENTAL

Sample Preparation

The new compound $Ce_2O(NO_3)_6 \cdot 8H_2O$ was synthesized from a solution of ceria in concentrated nitric acid, partially evaporated at 40°C, in ambient atmosphere. The main difficulty in obtaining pure ceric nitrate solution is preventing the reduction of Ce^{4+} into $Ce3^+$ during the reaction of CeO_2 with boiling nitric acid solution. This requires a highly soluble oxide, which is not commonly the case for available products. Consequently, the first stage of the synthesis is related to the preparation of hydrous ceria with very small crystallites. It was obtained, at room temperature, from 200 ml of 0.1 *M* neutral cerous nitrate solution into which was added dropwise 100 ml of 1 *M* sodium hydroxide solution. The violet precipitate was decanted, repeatedly washed with water and alcohol, filtered, and then dried at room temperature under reduced pressure for about 24 hr. From thermogravimetric analysis its composition was found to be $CeO_2 \cdot 2.4H_2O$. This oxide is characterized by a mean crystallite size of 30 Å deduced from X-ray diffraction line profile analysis by means of a Williamson–Hall plot (14). One gram of

0022-4596/94 $6.00

hydrous ceria was completely soluble, within a few minutes, in 20 ml of concentrated nitric acid boiling in a closed vessel. From this solution, kept in an oven at 40°C, a red crystalline phase or a vitreous phase is formed after a few days. In fact, the vitreous phase is unstable, as shown by its rapid crystallization as soon as it is stirred. The compound is hygroscopic and a further study has shown that, under a water pressure of 10 Torr, the water content can increase up to two additional H_2O molecules. The Ce^{4+} content was determined by titration, with Mohr's salt and ferroin indicator, and NO_3^- content by the Dewarda method. The values obtained, 32.97 and 43.72% respectively, correspond to a ratio NO_3^-/Ce^{4+} of 2.997. They are in agreement with the chemical formula $Ce_2O(NO_3)_6 \cdot 10H_2O$. This overstoichiometry in water molecules was clearly shown by thermogravimetric analysis, after the compound was kept in nitrogen atmosphere at room temperature for a few hours. The stable phase contains $8H_2O$, as shown by a weight loss of 57.60% for its conversion into CeO_2. This value compares well with the theoretical value, 57.62%. It can be concluded that the global chemical formula of this new compound is $Ce_2O(NO_3)_6 \cdot 8H_2O$.

X-ray Powder Diffraction Data Collection

X-ray powder diffraction data for the new cerium oxide precursor were collected with a D500 Siemens powder diffractometer using the Bragg–Brentano geometry, whose features were reported elsewhere (15). Pure Cu$K\alpha_1$ radiation (1.54059 Å) was produced with an incident beam curved-crystal germanium monochromator. The alignment of the diffractometer was checked by means of standard reference materials and the zero error was measured as less than 0.005°(2θ). For the microstructural analysis of cerium oxide the diffraction pattern was scanned over the angular range 24 to 145°(2θ), with a step length of 0.04°(2θ). The counting time was 62 sec step^{-1} to 64.52° and 124 sec step^{-1} from 64.56° to the end of the scan. The extraction of peak positions, breadths, and diffraction line shapes was carried out with the Socabim fitting program FIT available in the DIFFRAC-AT software package supplied by Siemens.

The high-temperature X-ray diffraction experiments (HTRXD) were carried out by using a INEL (CPS120) curved position-sensitive detector. The detector was used in a semifocusing geometry by reflection, described elsewhere (16). Monochromatic Cu$K\alpha_1$ radiation was selected using an incident-beam curved quartz monochromator with asymmetric focusing (short focal distance = 130 mm, long focal distance = 510 mm). The stationary powder sample is located at the center of the goniometer and intercepts the convergent X-ray beam. A fixed θ_i angle of 6° between the incident beam and the surface of the sample was selected. Samples were located in a monitored high-temperature device (Rigaku). Experiments were carried out under vacuum of 1.5 Pa with the following conditions: 12 hr at room temperature, heating rate of 3°C hr^{-1} between room temperature and 200°C, and 15°C hr^{-1} in the range 200–500°C. To ensure satisfactory counting statistics an interval time of 3240 sec between two successive powder diffraction patterns was selected, including a counting time of 3000 sec.

Thermogravimetric Analysis

Thermogravimetric analysis was carried out with a thermobalance of McBain type. Powder samples of about 70 mg were spread evenly in a large sample holder to avoid mass effects and to reproduce as much as possible the same conditions as used in the HTRXD study.

Powder Diffraction Pattern Indexing

As described above the new Ce(IV) compound is essentially obtained in a polycrystalline form with low stability. Nevertheless, precise powder diffraction data could be collected and indexed with the program DICVOL91 (17), which is based on the variation of direct parameters by means of a successive dichotomy procedure. An absolute error on observed lines of 0.03°(2θ) was attributed to the input data. From the first 20 lines a monoclinic solution was proposed with satisfactory figures of merit [M_{20} = 75, F_{20} = 167(0.0031, 39)]. The complete dataset was reviewed by means of the computer program NBS*AIDS83 (18). From this evaluation, the cell dimensions are a = 8.7233(8), b = 8.9397(8), c = 13.981(1) Å, β = 94.909(7)°, and V = 1086.3(1) Å^3 with M_{20} = 70 and F_{30} = 152(0.0046, 43). Systematic absences ($h0l$, l odd; and $0k0$, k odd) are consistent with the monoclinic $P2_1/c$ space group. The X-ray powder diffraction data are given in Table 1.

Structure Determination and Refinement

From a careful examination by optical microscopy of the polycrystalline phase $Ce_2O(NO_3)_6 \cdot 8H_2O$, a crystal (0.42 × 0.35 × 0.20 mm) could be isolated and sealed into a capillary tube. Diffraction data collection was carried out with an Enraf–Nonius CAD-4 diffractometer, using graphite-monochromated Mo$K\alpha$ radiation. Cell constants, determined by the least-squares treatment of 24 reflections with 2θ values between 16.2 and 20.7°, were in agreement with the solution derived from the automatic indexing of the powder diffraction pattern. One set of intensities ($h: 0 \rightarrow 11$, $k: 0 \rightarrow 11$, $l: \bar{17} \rightarrow 17$) was collected at room temperature by a θ–2θ scanning technique to give 2331 unique reflections with $\sin\theta/\lambda \leq 0.6831$ Å^{-1}. Within this set, 2091 reflections were considered as observed by means of the criterion $I > 3\sigma(I)$. Data were corrected for

TABLE 1
X-ray Powder Diffraction Data for $Ce_2O(NO_3)_6(H_2O)_6 \cdot 2H_2O$

hkl	$2\theta_{obs}$ (°)	$2\theta_{calc}$ (°)	d_{obs} (Å)	I_{obs}
100	10.170	10.169	8.69	19
011	11.760	11.753	7.52	100
002	12.701	12.699	6.96	4
$\bar{1}11$	15.186	15.203	5.83	1
$\bar{1}02$	15.592	15.596	5.68	10
111	15.917	15.920	5.56	40
012	16.122	16.119	5.49	1
102	16.958	16.967	5.22	12
$\bar{1}12$	18.492	18.498	4.794	3
020	19.848	19.847	4.470	9
200	20.418	20.420	4.346	10
021	20.851	20.854	4.257	6
013	21.543	21.548	4.122	7
120	22.354	22.348	3.974	7
$\bar{1}21$	23.013	23.007	3.862	9
$\bar{2}11$		23.140		
$\bar{1}13$	23.157	23.157	3.838	46
$\bar{2}02$		23.160		
022	23.627	23.632	3.763	2
211	24.088	24.099	3.962	1
113	24.581	24.582	3.619	3
202	25.043	25.044	3.553	3
$\bar{1}22$	25.342	25.340	3.512	6
004	25.554	25.558	3.483	5
122	26.227	26.224	3.395	8
$\bar{1}04$	26.730	26.728	3.332	7
014	27.462	27.464	3.245	7
023	27.675	27.679	3.221	2
$\bar{2}13$	28.670	28.678	3.111	4
$\bar{2}21$		28.955		
$\bar{1}23$	28.970	28.969	3.080	3
221	29.743	29.739	3.001	4
114		30.131		
123	30.152	30.138	2.961	1
031	30.662	30.656	2.913	10
$\bar{2}22$		30.682		
300	30.842	30.839	2.897	5
213	30.996	30.996	2.883	7
$\bar{2}04$	31.492	31.490	2.838	8
222	32.163	32.157	2.781	3
131		32.557		
024	32.566	32.568	2.747	21
$\bar{3}11$		32.576		
032	32.656	32.659	2.740	4
$\bar{2}14$	33.085	33.083	2.705	2
$\bar{1}24$	33.513	33.514	2.672	9
311		33.632		
015	33.662	33.668	2.660	4
$\bar{1}32$	33.951	33.948	2.638	3
312		33.967		
204	34.330	34.321	2.610	3
$\bar{1}15$	34.425	34.418	2.603	1
124	34.883	34.882	2.570	2
033	35.778	35.775	2.508	2
214		35.802		
$\bar{3}12$	35.980	35.979	2.4941	2
115	36.082	36.083	2.4873	5
$\bar{3}13$		36.504		
230	36.531	36.533	2.4577	3
$\bar{2}31$		36.798		
$\bar{1}33$	36.805	36.809	2.4400	2
320	36.948	36.945	2.4309	4
231	37.458	37.435	2.3990	1
133	37.762	37.761	2.3804	3

Lorentz and polarization effects and extinction corrections were applied. Absorption corrections were based on a ψ scan program; the maximum and minimum transmission relative factors were 0.9996 and 0.5666, respectively. Atomic scattering factors were taken from "International Tables for X-ray Crystallography." All calculations were performed on a DEC micro VAX 3100 computer with the *MolEN* system of programs (19).

Direct methods (program MULTAN) yielded the position of the cerium atom, which was also confirmed by the Patterson method. The positions of the 17 remaining nonhydrogen atoms were obtained from successive Fourier maps. The list of interatomic distances showed that among them 12 corresponded to three independent nitrate groups. One oxygen atom, located on the inversion center, cannot belong to a water molecule or a hydroxyl group and must be considered as an oxo bridge since it is bonded to two cerium atoms. Taking into account the oxidation state IV for the cerium atom, it was assumed that the four remaining atoms corresponded to water molecules. Consequently, the chemical formula $Ce_2O(NO_3)_6 \cdot 8H_2O$ can be proposed; it is in agreement with the chemical analysis and TG measurements. The R and wR values, including anisotropic thermal parameters, were 0.023 and 0.038, respectively. The height of the

TABLE 2
Crystallographic Data for $Ce_2O(NO_3)_6(H_2O)_6 \cdot 2H_2O$

Empirical formula	$Ce_2O(NO_3)_6 \cdot 8H_2O$
Molecular weight	812.39
Crystal system	Monoclinic
Space group	$P2_1/c$
a (Å)	8.7233(8)
b (Å)	8.9397(8)
c (Å)	13.981(1)
β (°)	94.909(7)
V (Å^3)	1086.3(1)
Z	2
Radiation (Å)	0.71069
Data collection	$h, k, \pm l$
No. observations	2091
No. variables	161
R	0.023
wR	0.038

TABLE 3
Positional Parameters and Their Equivalent Isotropic Thermal Parameters with Their Estimated Standard Deviations

Atom	x	y	z	B_{eq} (Å^2)
Ce	0.64713(2)	0.03059(2)	0.39539(1)	1.491(4)
$O1_1$	0.8424(3)	0.1231(3)	0.5170(2)	2.745(5)
$O1_2$	0.6492(3)	0.2729(3)	0.5049(2)	3.25(5)
$O1_3$	0.8374(4)	0.3179(4)	0.6108(2)	4.40(7)
$O2_1$	0.4316(3)	0.1929(3)	0.3349(2)	2.23(4)
$O2_2$	0.3839(3)	−0.0407(3)	0.3134(2)	2.60(5)
$O2_3$	0.2021(3)	0.1218(4)	0.2788(2)	3.66(6)
$O3_1$	0.7722(3)	−0.1787(3)	0.4968(2)	2.93(5)
$O3_2$	0.6261(3)	−0.2380(3)	0.3703(2)	2.89(5)
$O3_3$	0.7450(6)	−0.4119(4)	0.4537(3)	7.3(1)
N1	0.7761(3)	0.2438(3)	0.5449(2)	2.56(5)
N2	0.3341(3)	0.0924(4)	0.3076(2)	2.22(5)
N3	0.7159(4)	−0.2807(4)	0.4424(2)	3.47(7)
O	0.500	0.000	0.500	2.09(6)
Ow1	0.9068(3)	−0.0355(3)	0.3482(2)	3.04(6)
Ow2	0.6432(3)	−0.0087(3)	0.2184(2)	2.68(5)
Ow3	0.7480(3)	0.2495(3)	0.3187(2)	2.65(5)
Ow4	0.9728(3)	−0.1234(4)	0.1514(3)	4.34(7)

Note. Anisotropically refined atoms are given in the form of the isotropic equivalent displacement parameter defined as $(4/3)[a^2B(1, 1) + b^2B(2, 2) + c^2B(3, 3) + ab(\cos\gamma)B(1, 2) + ac(\cos\beta)B(1, 3) + bc(\cos\alpha)B(2, 3)]$.

residual peaks observed on a final difference Fourier map ranged from 0.139 to 0.819 e Å^{-3}, but none of them could be ascribed to hydrogen atoms. Crystallographic data and final atomic parameters with equivalent temperature factors are given in Tables 2 and 3, respectively. $O1_1$ to $O3_3$ correspond to the oxygen atoms of nitrate groups, O to the oxo bridge and Ow_1 to Ow_4 to water molecules. Selected bond distances and angles are listed in Table 4.

DESCRIPTION OF THE STRUCTURE

The crystal structure of this new compound can be described as consisting of isolated dimer units linked together through hydrogen bonds. These units, with formula $Ce_2O(NO_3)_6(H_2O)_6$, are formed by two equivalent 10-fold cerium(IV) polyhedra connected by an oxo bridge, as shown in Fig. 1. The other water molecules are located between these dimer units.

Cerium Polyhedra

The cerium atoms are 10-fold coordinated. They are bonded to three bidendate nitrate groups, three water molecules, and an oxygen atom. The different nature of these ligands generates very different Ce–O distances and explains the distortion of the polyhedron. Indeed, the Ce–O distances range from 2.0451(2) to 2.652(3) Å. The mean value of 2.455 Å is in accordance with that calculated by the bond valence method (20) for 10-fold coordinated Ce(IV), namely 2.416 Å. This polyhedron (Fig. 2) is built from 16 triangular faces, the vertex being common to 6, 5, or 4 faces. This 10-fold coordination has also been found in Ce(IV) and Th(IV) salts, as in guanidinium or sodium pentacarbonatocerate (21, 22), in which the mean Ce–O distances (2.448 and 2.437 Å, respectively) are in good agreement with the results reported here.

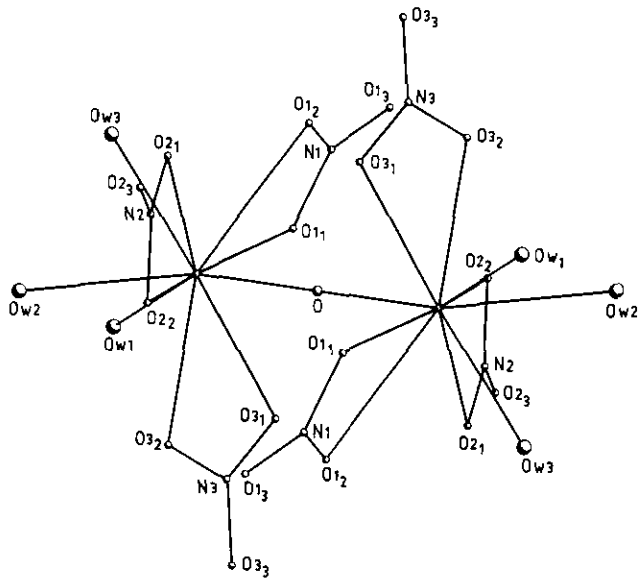

FIG. 1. The dimer unit $Ce_2O(NO_3)_6(H_2O)_6$.

Nitrate Groups

The three nitrate groups act as bidentate ligands. Two of them (N2 and N3) are bidentate symmetric [class I_{2b} reported by Leclaire (23)]. In that case, the bond distances N2–$O2_3$ and N3–$O3_3$ (mean value, 1.211 Å) are signifi-

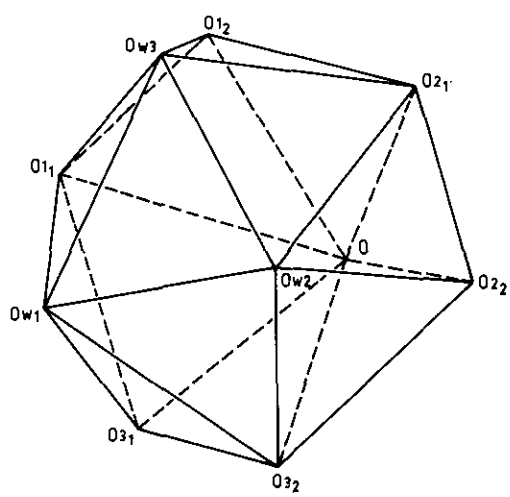

FIG. 2. The cerium(IV) coordination in $Ce_2O(NO_3)_6(H_2O)_6 \cdot 2H_2O$.

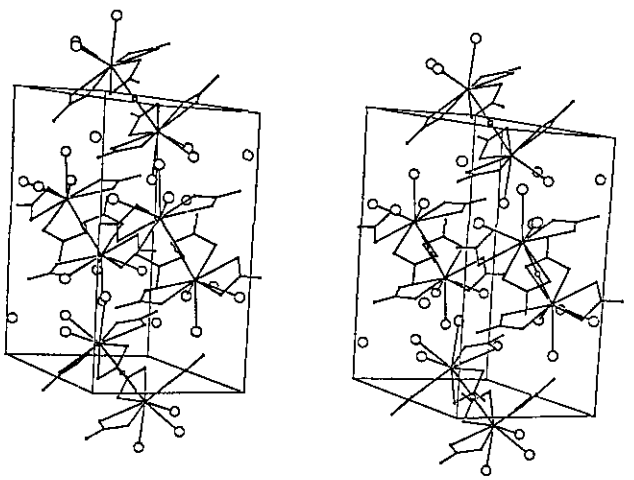

FIG. 3. Stereoscopic view of the unit cell contents, with *a* horizontal and *c* vertical. Large circles correspond to water molecules.

cantly shorter than the other N–O distances (mean value, 1.270 Å). The remaining nitrate group (N1) is bidentate asymmetric ($N1–O1_1$ = 1.300 Å and $N1–O1_2$ = 1.224 Å). In all cases, the angle formed by the nitrogen and the two bonded oxygen atoms is significantly smaller than the two others and the thermal parameter of the terminal oxygen atom is also higher.

Water Molecules

Three independent water molecules (Ow1, Ow2, and Ow3) are linked to the cerium atom with distances ranging from 2.432 to 2.496 Å. The other independent water molecule (Ow4) lies between the dimer units as shown in Fig. 3. Attempts to locate hydrogen atoms failed, but taking into account Baur's criteria (24), two hydrogen bonds by water molecule are possible (see Table 4). The dimer units are linked together through hydrogen bonds between two water molecules or between a water molecule and a nitrate group. Two dimer units could be linked through hydrogen bonds directly or through the nonbonded water molecule.

TABLE 4
Selected Bond Distances (Å) and Angles (°)

Within the cerium polyhedron

Ce	$O1_1$	2.446(2)	Ce	O	2.0451(2)
Ce	$O1_2$	2.652(3)	Ce	Ow1	2.484(3)
Ce	$O2_1$	2.466(2)	Ce	Ow2	2.496(3)
Ce	$O2_2$	2.557(3)	Ce	Ow3	2.432(3)
Ce	$O3_1$	2.537(3)			
Ce	$O3_2$	2.431(3)			

Within the nitrate groups

$O1_1$	N1	1.300(4)	$O2_1$	N2	1.273(4)	$O3_1$	N3	1.260(4)
$O1_2$	N1	1.224(4)	$O2_2$	N2	1.268(4)	$O3_2$	N3	1.280(4)
$O1_3$	N1	1.221(4)	$O2_3$	N2	1.215(4)	$O3_3$	N3	1.208(5)

$O1_1$	N1	$O1_2$	116.6(3)	$O2_1$	N2	$O2_2$	115.2(3)
$O1_1$	N1	$O1_3$	120.0(3)	$O2_1$	N2	$O2_3$	122.5(3)
$O1_2$	N1	$O1_3$	123.4(3)	$O2_2$	N2	$O2_3$	122.3(3)

$O3_1$	N3	$O3_2$	116.1(3)
$O3_1$	N3	$O3_3$	123.8(4)
$O3_2$	N3	$O3_3$	120.0(4)

Possible hydrogen bonds

$O1_1{}^a$	Ow1	2.872(4)	$O1_3{}^b$	Ow2	2.912(4)
Ow4	Ow1	2.965(5)	$O2_1{}^c$	Ow2	2.831(3)
$O1_1{}^a$	Ow1	Ow4	109.8(1)	$O1_3{}^b$	Ow2	$O2_1{}^c$	123.2(1)
$O2_2{}^d$	Ow3	2.809(4)	$O1_3{}^b$	Ow4	3.010(5)
Ow4^e	Ow3	2.687(4)	$O2_3{}^c$	Ow4	2.954(4)
$O2_2{}^d$	Ow3	Ow4^e	97.8(1)	$O1_3{}^b$	Ow4	$O2_3{}^c$	123.8(1)

Note. Symmetry codes: [a] 2 − x, −y, 1 − z; [b] x, 1/2 − y, z − 1/2; [c] 1 − x, y − 1/2, 1/2 − z; [d] 1 − x, 1/2 + y, 1/2 − z; [e] 2 − x, 1/2 + y, 1/2 − z. Numbers in parentheses are estimated standard deviations in the last significant digits.

These hydrogen bonds ensure the continuity of the structure.

THERMAL ANALYSIS AND MICROSTRUCTURE OF CERIUM OXIDE

Figure 4 shows a three-dimensional representation of the successive diffraction patterns during the decomposition of the new cerium oxide nitrate in the range 20–500°C. It shows that, under vacuum, the decomposition of the precursor into the final product CeO_2 takes place in three steps. Table 5 summarizes the main characteristics of the complete thermal decomposition as deduced from HTXRD and TG analyses. The two first stages correspond to the formation of two new phases, $Ce_2O(NO_3)_6 \cdot 3H_2O$ and $Ce_2O(NO_3)_6$. We may notice that the trihydrate phase is formed at room temperature. The pattern of the anhydrous phase consists of a few broad lines. The latter compound with low crystallinity leads to CeO_2, whose diffraction pattern exhibits considerable broadened diffraction lines arising from the very small diffracting domains formed during the thermal decomposition. The growing of these crystallites with temperature is clearly seen in Fig. 4 and a study of the microstructure of the nanoscale particles of CeO_2 is reported below. From Table 5 it can be seen that there is a large discrepancy between the temperature at the end of the structural transformation (180°C) and that at the end of weight loss observed at 400°C. This effect is interpretated by the slow release of gases (NO, NO_2, and O_2) strongly adsorbed on the finely dispersed oxide powder. The difference between the starting temperatures of these ranges can be explained by the inaccuracy on the weak integrated intensity of the diffraction lines of the anhydrous cerium oxide nitrate.

Precise powder diffraction data for $Ce_2O(NO_3)_6 \cdot 3H_2O$ were collected under vacuum, at room temperature, with a diffractometer equipped with a diffracted beam monochromator ($CuK\alpha_{12}$). The diffraction lines are broadened [$0.10°(2\theta) \leq$ FWHM $\leq 0.25°(2\theta)$] by comparison with the instrumental resolution function of the diffractometer, for which an average FWHM value of $0.08°(2\theta)$ is observed in the low angle region. Nevertheless, the indexing of the powder diffraction pattern by the program DICVOL91 (17) has been successful. The first 20 lines were indexed on the basis of a triclinic cell with the figures of merit $M_{20} = 26$ and $F_{20} = 50(0.013, 31)$. This solution was used for reviewing the complete powder diffraction data by means of the program NBS*AIDS83 (18). From this evaluation of data quality and refinement, the cell dimensions were found to be $a = 7.937(5)$, $b = 8.452(4)$, $c = 7.083(4)$ Å, $\alpha = 103.61(4)$, $\beta = 104.16(5)$, $\gamma = 83.01(5)°$, $V = 446.7(3)$ Å^3. The final figures of merit are $M_{20} = 26$ and $F_{25} = 39(0.016, 40)$. The list of observed and calculated peak positions is given in Table 6.

The microstructure of cerium oxide annealed at 600°C for 24 hr has been investigated by diffraction line broadening analysis after total pattern decomposition. The integral breadths (=area/peak intensity) of 16 reflections were obtained from the fitting of Voigt functions, available in the Socabim program FIT, to the individual Bragg compo-

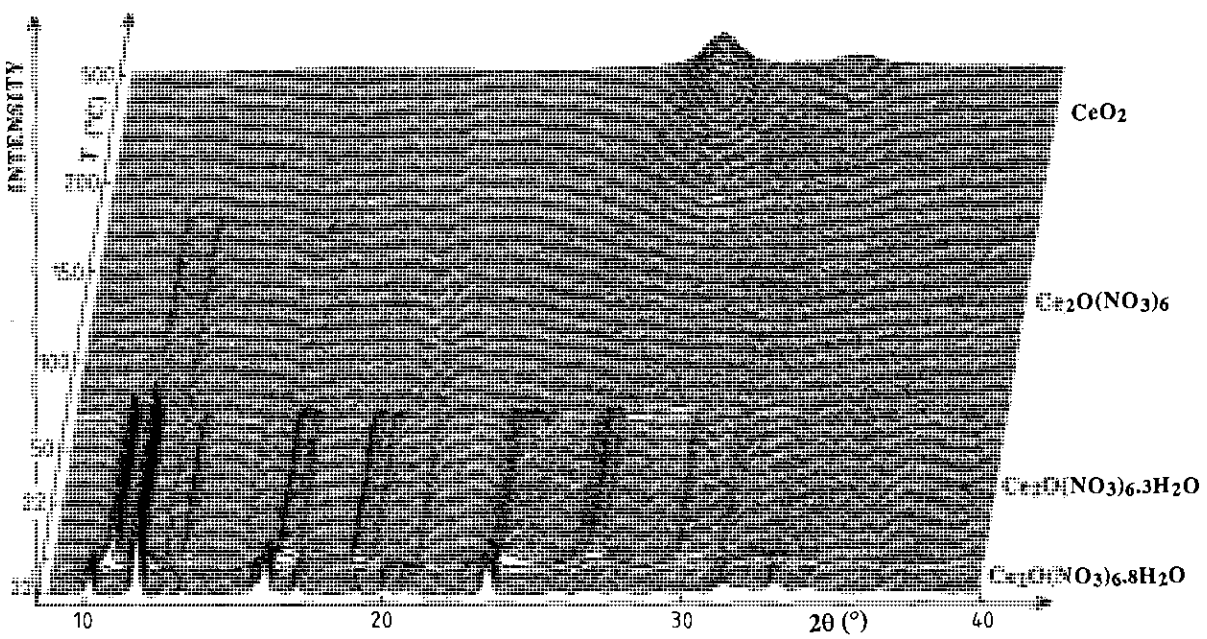

FIG. 4. HTXRD plot of $Ce_2O(NO_3)_6(H_2O)_6 \cdot 2H_2O$ in vacuum (room temperature for 12 hr; 3°C h^{-1} between room temperature and 200°C; 15°C h^{-1} in the range 200–500°C).

TABLE 5
The Successive Stages of the Thermal Decomposition of $Ce_2O(NO_3)_6(H_2O)_6 \cdot 2H_2O$ in Vacuum

Stage	Transformation	$\Delta m/m_0$ (%) (observed)	$\Delta m/m_0$ (%) (calculated)	Temperature range (°C)(HTRXD)	Temperature range (°C)(TG)
1	$Ce_2O(NO_3)_6(H_2O)_6 \cdot 2H_2O \rightarrow Ce_2O(NO_3)_6 \cdot 3H_2O + 5H_2O$	11.2	11.28	22	22
2	$Ce_2O(NO_3)_6 \cdot 3H_2O \rightarrow Ce_2O(NO_3)_6 + 3H_2O$	6.7	6.70	50–72	50–80
3	$Ce_2O(NO_3)_6 \rightarrow 2CeO_2 + xNO + (6 - x)NO_2 + [(3 + x)/2]O_2$	39.6	39.64	140–180	80–400

nents. The complete procedure used in the analysis has been recently reported (12, 25). Correction for instrumental contribution was based on the properties of the Voigt function (25), which was appropriate since the observed Voigt parameters $\Phi(=\text{FWHM}/\beta)$ [$\langle\Phi_{obs}\rangle = 0.70(3)$] lie between the Lorentzian ($\Phi = 0.634$) and the Gaussian ($\Phi = 0.939$) limits for all investigated lines. To correct the observed integral breadths for instrumental contribution, the breadths of the instrumental lines were obtained from a sample of an annealed BaF_2 standard material described elsewhere (15). The Williamson–Hall plot (14), in which the corrected integral breadths β_f^* in reciprocal units ($=\beta_f(2\theta)\cos\theta/\lambda$) is ploted as a function of d^* ($=2\sin\theta/\lambda$) was obtained. From this plot it was apparent that line broadening was essentially isotropic and that the slope of the least-squares line through the points was slightly positive. As shown before, β_f^* is Voigtian, so if it is assumed that the Lorentzian component, $\beta_L = \beta_S$, is due to size effects and that the Gaussian component, $\beta_G = \beta_D$, arises from microstrains, therefore the "average" Halder–Wagner size-strain plot (26) can be used for a separation of size/strain effects. According to Langford (25) (Eqs. 22 and 23), the mean apparent size (ε) and microstrain parameter (η) are derived from the equation

$$(\beta_f^*/d^*)^2 = \varepsilon^{-1}\beta_f^*/(d^*)^2 + (\eta/2)^2.$$

The plot $(\beta_f^*/d^*)^2$ versus $\beta_f^*/(d^*)^2$ for CeO_2, at 600°C, is shown Fig. 5. From a least-squares fit, the slope of the straight line gives the mean apparent size $\langle\varepsilon\rangle = 207(4)$ Å and the intercept the rms strain [$e = \eta/2\sqrt{(2\pi)}$] $\langle e\rangle = 8.79(3) \times 10^{-4}$. This result confirms the small microstrain effect. On the other hand, owing to the diffraction-line broadening isotropy, the crystallite shape of CeO_2 can be described, on average, by a sphere of mean diameter $\langle D\rangle$ ($=4\langle\varepsilon\rangle/3$) = 276(7) Å.

TABLE 6
X-ray Powder Diffraction Data for $Ce_2O(NO_3)_6 \cdot 3H_2O$

hkl	$2\theta_{obs}$ (°)	$2\theta_{calc}$ (°)	d_{obs} (Å)	I_{obs}
010	10.753	10.786	8.22	77
100	11.521	11.516	7.67	100
001	13.154	13.185	6.73	16
$0\bar{1}1$	15.207	15.163	5.82	5
110		15.255		
$\bar{1}10$	16.320	16.355	5.43	25
$\bar{1}11$	16.649	16.677	5.32	30
011	18.763	18.781	4.725	26
$10\bar{1}$	19.403	19.406	4.571	15
$\bar{1}11$	20.850	20.872	4.257	12
$1\bar{1}1$	21.227	21.224	4.182	6
020	21.663	21.670	4.099	7
$02\bar{1}$	22.863	22.869	3.886	6
$11\bar{1}$	23.248	23.239	3.823	12
$\bar{1}2\bar{1}$	23.540	23.550	3.776	38
$\bar{2}01$	23.970	23.972	3.709	24
$\bar{2}11$	24.444	24.436	3.639	17
$\bar{1}20$	25.311	25.302	3.516	5
$1\bar{1}2$	26.063	26.053	3.416	14
$0\bar{1}2$	26.480	26.451	3.363	35
$\bar{1}02$		26.484		
021	27.824	27.806	3.204	7
$20\bar{1}$	29.297	29.253	3.046	16
$\bar{2}2\bar{1}$		29.336		
$\bar{1}21$	29.611	29.589	3.014	6
$\bar{1}22$	29.982	29.960	2.978	11
$2\bar{1}2$	30.576	30.550	2.921	3
$02\bar{2}$		30.600		
$2\bar{1}1$	30.835	30.808	2.897	14
012		30.856		

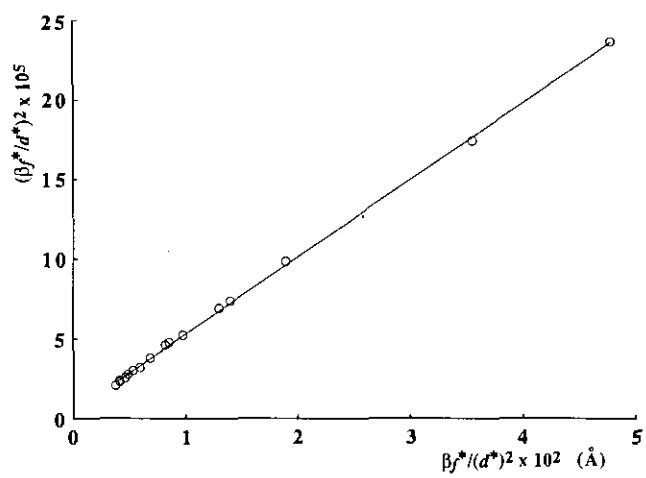

FIG. 5. "Average" Halder–Wagner size/strain plot for CeO_2 annealed at 600°C for 25 hr.

CONCLUDING REMARKS

From finely dispersed hydrated cerium oxide, it has been possible to stabilize a Ce(IV) compound containing nitrate groups. The structure solution reported in this work shows that the compound formed in the CeO_2–HNO_3–H_2O system has the chemical formula $Ce_2O(NO_3)_6(H_2O)_6 \cdot 2H_2O$. It can be noted that this new compound presents a global formula close to that obtained by Meyer and Jacoby (2) and formulated as a hydroxide nitrate $Ce(OH)(NO_3)_3 \cdot 3H_2O$. The structural results reported in the present study demonstrates that the new cerium(IV) nitrate compound is an oxide nitrate. This result should give valuable structural references for interpreting EXAFS spectra obtained in the course of the study of polymeric species resulting from the hydrolysis of hydrated Ce^{4+} in solution. Moreover, owing to the high content in water molecules and the low thermal stability of nitrate groups, CeO_2 with nanoscale diffracting domains is formed at a low temperature after a two-step decomposition process. Finally, the study has shown that the oxide nitrate is not a very stable phase, and other decomposition mechanisms by changing environmental conditions, e.g., water pressure, are being investigated at present.

REFERENCES

1. W. P. Hsu, L. Rönnquist and E. Matijevic, *Langmuir.* **4,** 31 (1988).
2. R. J. Meyer and R. Jacoby, *Z. Anorg. Chem.* **27,** 359 (1901).
3. E. Staritky, *Anal.Chem.* **28,** 12, 2022 (1956).
4. D. L. Rogachev, M. A. Porai-Koshits, V. Ya. Kuznetsov, and L. M. Dikareva, *J. Struct. Chem. (URSS)* **15,** 397 (1974).
5. O. Lindgren, *Acta Chem. Scand. A* **31,** 453 (1977).
6. O. Lindgren, *Acta Crystallogr. Sect. B* **32,** 3347 (1976).
7. O. Lindgren, *Acta Chem. Scand. A* **31,** 163 (1977).
8. G. Lundgren, *Arkiv Kemi* **10,** 183 (1957).
9. H. Cyao and Y. F. Yu Uao, *J. Catal.* **86,** 254 (1984).
10. E. Su, C. Montreuil and W. Rothschild, *Appl. Catal.* **17,** 75 (1985).
11. D. Louër, J. P. Auffrédic, J. I. Langford, D. Ciosmak, and J. C. Niepce, *J. Appl. Crystallogr.* **16,** 183 (1983).
12. J. I. Langford, A. Boultif, J. P. Auffrédic, and D. Louër, *J. Appl. Crystallogr.* **26,** 22 (1993).
13. N. Guillou, J. P. Auffrédic, M. Louër, and D. Louër, *J. Solid State Chem.* **106,** 295 (1993).
14. G. K. Williamson and W. H. Hall, *Acta Metall.* **1,** 22 (1953).
15. D. Louër and J. I. Langford, *J. Appl. Crystallogr.* **21,** 430 (1988).
16. J. Plévert, J. P. Auffrédic, M. Louër, and D. Louër, *J. Mater. Sci.* **24,** 1913 (1989).
17. A. Boultif and D. Louër, *J. Appl. Crystallogr.* **24,** 987 (1991).
18. A. D. Mighell, C. R. Hubbard, and J. K. Stalick, "NBS*AIDS80: A FORTRAN Program for Crystallographic Data Evaluation." NBS (U.S.) Tech. Note 1141.(NBS*AIDS83 is an expanded version of NBS*AIDS80), 1981.
19. "MolEN, an Interactive Structure Solution Procedure." Enraf-Nonius, Delft, The Netherlands, 1990.
20. I.D. Brown and K. K. Wu, *Acta Crystallogr. Sect. B* **32,** 1957 (1976).
21. S. Voliotis, A. Rimsky, and J. Faucherre, *Acta Crystallogr. Sect. B* **31,** 2607 (1975).
22. S. Voliotis and A. Rimsky, *Acta Crystallogr. Sect. B* **31,** 2620 (1975).
23. A. Leclaire, *J. Solid State Chem.* **28,** 235 (1979).
24. W. H. Baur, *Acta Crystallogr.* **17,** 863 (1964).
25. J. I. Langford, *in* "Accuracy in Powder Diffraction II." (E. Prince and J. K. Stalick, Eds.) NIST Spec. Public. 846, pp. 110–126 (1992).
26. N. C. Halder and C. N. J. Wagner, *Acta Crystallogr.* **20,** 312 (1966).